

1 **Interactions of organosulfates with water vapor under sub- and supersaturated**  
2 **conditions**

3  
4 Chao Peng,<sup>1,2</sup> Patricia N. Razafindrambinina,<sup>3</sup> Kotiba A. Malek,<sup>4</sup> Lanxiadi Chen,<sup>1,2,7</sup> Weigang  
5 Wang,<sup>5</sup> Ru-Jin Huang,<sup>6</sup> Yuqing Zhang,<sup>1,2</sup> Xiang Ding,<sup>1,2</sup> Maofa Ge,<sup>5</sup> Xinming Wang,<sup>1,2</sup> Akua A.  
6 Asa-Awuku,<sup>3,4</sup> and Mingjin Tang<sup>1,2,7,\*</sup>

7  
8 <sup>1</sup> State Key Laboratory of Organic Geochemistry, Guangdong Key Laboratory of Environmental  
9 Protection and Resources Utilization, and Guangdong-Hong Kong-Macao Joint Laboratory for  
10 Environmental Pollution and Control, Guangzhou Institute of Geochemistry, Chinese Academy of  
11 Sciences, Guangzhou 510640, China

12 <sup>2</sup> CAS Center for Excellence in Deep Earth Science, Guangzhou 510640, China

13 <sup>3</sup> Department of Chemistry and Biochemistry, College of Computer, Mathematical and Natural  
14 Sciences, University of Maryland, College Park, MD 20742, USA

15 <sup>4</sup> Department of Chemical and Biomolecular Engineering, A. James Clark School of Engineering,  
16 University of Maryland, College Park, MD 20742, USA

17 <sup>5</sup> State Key Laboratory for Structural Chemistry of Unstable and Stable Species, Beijing National  
18 Laboratory for Molecular Sciences, CAS Research/Education Center for Excellence in Molecular  
19 Sciences, Institute of Chemistry, Chinese Academy of Sciences, Beijing 100190, China

20 <sup>6</sup> Key Laboratory of Aerosol Chemistry and Physics, State Key Laboratory of Loess and  
21 Quaternary Geology, Institute of Earth and Environment, Chinese Academy of Sciences, Xi'an  
22 710061, China

23 <sup>7</sup> University of Chinese Academy of Sciences, Beijing 100049, China

24

25 \*Correspondence: Mingjin Tang ([mingjintang@gig.ac.cn](mailto:mingjintang@gig.ac.cn))

26

27

28 **Abstract**

29 Organosulfates (OS) are important constituents of secondary organic aerosols, but their  
30 hygroscopic properties and cloud condensation nucleation (CCN) activities have not been well  
31 understood. In this work we employed three complementary techniques to characterize interactions  
32 of several OS with water vapor under sub- and supersaturated conditions. A vapor sorption  
33 analyzer was used to measure mass changes of OS samples with RH (0-90%); among the 11  
34 organosulfates examined, only sodium methyl sulfate (methyl-OS), sodium ethyl sulfate (ethyl-  
35 OS), sodium octyl sulfate (octyl-OS) and potassium hydroxyacetone sulfate were found to  
36 deliquesce as RH increased, and their mass growth factors at 90% RH were determined to be  
37  $3.65 \pm 0.06$ ,  $3.58 \pm 0.02$ ,  $1.59 \pm 0.01$  and  $2.20 \pm 0.03$ . Hygroscopic growth of methyl-, ethyl- and octyl-  
38 OS aerosols was also studied using a humidity tandem differential mobility analyzer (H-TDMA);  
39 continuous hygroscopic growth was observed, and their growth factors at 90% RH were  
40 determined to be  $1.83 \pm 0.03$ ,  $1.79 \pm 0.02$  and  $1.21 \pm 0.02$ . We further investigated CCN activities of  
41 methyl-, ethyl- and octyl-OS aerosols, and their single hygroscopicity parameters ( $\kappa_{\text{ccn}}$ ) were  
42 determined to be  $0.459 \pm 0.021$ ,  $0.397 \pm 0.010$  and  $0.206 \pm 0.008$ . For methyl- and ethyl-OS aerosols,  
43  $\kappa_{\text{ccn}}$  values agree reasonably well with those derived from H-TDMA measurements ( $\kappa_{\text{gf}}$ ) with  
44 relative differences being <25%, whereas  $\kappa_{\text{ccn}}$  was found to be ~2.4 times larger than  $\kappa_{\text{gf}}$  for octyl-  
45 OS, likely due to both solubility limit and surface tension reduction.

46

## 47 **1 Introduction**

48 Secondary organic aerosol (SOA) contributes approximately 70% to the global atmospheric  
49 organic aerosols (Hallquist et al., 2009; Jimenez et al., 2009). SOA can affect the Earth's radiative  
50 forcing and climate directly by scattering and absorbing solar and terrestrial radiation, and also  
51 indirectly by acting as cloud condensation nuclei (CCN) or ice nucleating particles (Moise et al.,  
52 2015; Shrivastava et al., 2017). Consequently, it is important to understand the source, formation,  
53 and physicochemical properties of SOA (Pöschl, 2005; Jimenez et al., 2009; Noziere et al., 2015;  
54 Peng et al., 2020). However, SOA concentrations on the global scale are significantly  
55 underestimated by many modeling studies (Heald et al., 2005; Kanakidou et al., 2005; Ervens et  
56 al., 2011; McNeill et al., 2012; Shrivastava et al., 2017), indicating that there might exist unknown  
57 while important precursors and/or formation mechanisms of SOA.

58 Organosulfates (OS), which could contribute to the total mass of ambient organic aerosols by  
59 as much as 30%, may largely explain the discrepancy between observed and modeled global SOA  
60 budgets (Surratt et al., 2008; Tolocka and Turpin, 2012; Liao et al., 2015). A number of field  
61 measurements have observed significant amounts of OS in ambient aerosols in different regions  
62 over the globe (Froyd et al., 2010; Kristensen and Glasius, 2011; He et al., 2014; Hettiyadura et  
63 al., 2015; Riva et al., 2019; Wang et al., 2019a; Wang et al., 2019b; Zhang et al., 2019;  
64 Brüggemann et al., 2020; Wang et al., 2020). For example, the mass concentration of sodium  
65 methyl sulfate, the smallest organosulfate, was found to be 0.2-9.3 ng m<sup>-3</sup> in Centreville, Alabama  
66 (Hettiyadura et al., 2017). Hydroxyacetone sulfate, which may originate from both biogenic  
67 (Surratt et al., 2008) and anthropogenic emissions (Hansen et al., 2014), has been detected at  
68 various locations, such as the Arctic (1.27-9.56 ng m<sup>-3</sup>) (Hansen et al., 2014), Beijing (0.5-7.5 ng  
69 m<sup>-3</sup>) (Wang et al., 2018), Shanghai (1.8-2.3 ng m<sup>-3</sup>) (Wang et al., 2021), Xi'an (0.9-2.6 ng m<sup>-3</sup>)

70 (Huang et al., 2018), Centreville (1.5-14.3 ng m<sup>-3</sup>) (Hettiyadura et al., 2017) and Iowa City (4.8±1.1  
71 ng m<sup>-3</sup>) (Hughes and Stone, 2019). In addition, benzyl and phenyl sulfates were also ubiquitous in  
72 the troposphere, with reported concentrations up to almost 1 µg m<sup>-3</sup> (Kundu et al., 2013; Ma et al.,  
73 2014; Staudt et al., 2014; Huang et al., 2018).

74 As OS are ubiquitous in the troposphere, it is important to understand their hygroscopic  
75 properties and CCN activities in order to assess their environmental and climatic effects  
76 (Kanakidou et al., 2005; Moise et al., 2015; Tang et al., 2016; Tang et al., 2019a), especially  
77 considering that OS could contribute up to 30% of total mass of organic aerosols in the troposphere  
78 (Surratt et al., 2008; Tolocka and Turpin, 2012; Liao et al., 2015). However, to our knowledge,  
79 only two previous studies have explored their hygroscopic properties and CCN activities (Hansen  
80 et al., 2015; Estillore et al., 2016). Hansen et al. (2015) investigated hygroscopic growth and CCN  
81 activation of limonene-derived OS (with molecular weight of 250 Da) and their mixtures with  
82 ammonium sulfate. Hygroscopicity of pure limonene-derived OS was weak, and its hygroscopic  
83 growth factors were determined to be 1.0 at 80% RH and 1.2 at 93% RH (Hansen et al., 2015).  
84 Estillore et al. (2016) investigated hygroscopic growth of a series of OS, including potassium salts  
85 of glycolic acid sulfate, hydroxyacetone sulfate, 4-hydroxy-2,3-epoxybutane sulfate, and 2-  
86 butenediol sulfate, as well as sodium salts of benzyl sulfate, methyl sulfate, ethyl sulfate, and  
87 propyl sulfate. Continuous hygroscopic growth (i.e. without obvious deliquescence) was observed  
88 for these OS aerosols (Estillore et al., 2016); in addition, their hygroscopic growth factors at 85%  
89 RH were determined to vary between 1.29 and 1.50, suggesting that their hygroscopicity showed  
90 substantial variation. In summary, it is fair to state that hygroscopic properties and CCN activities  
91 of OS have not been well understood.

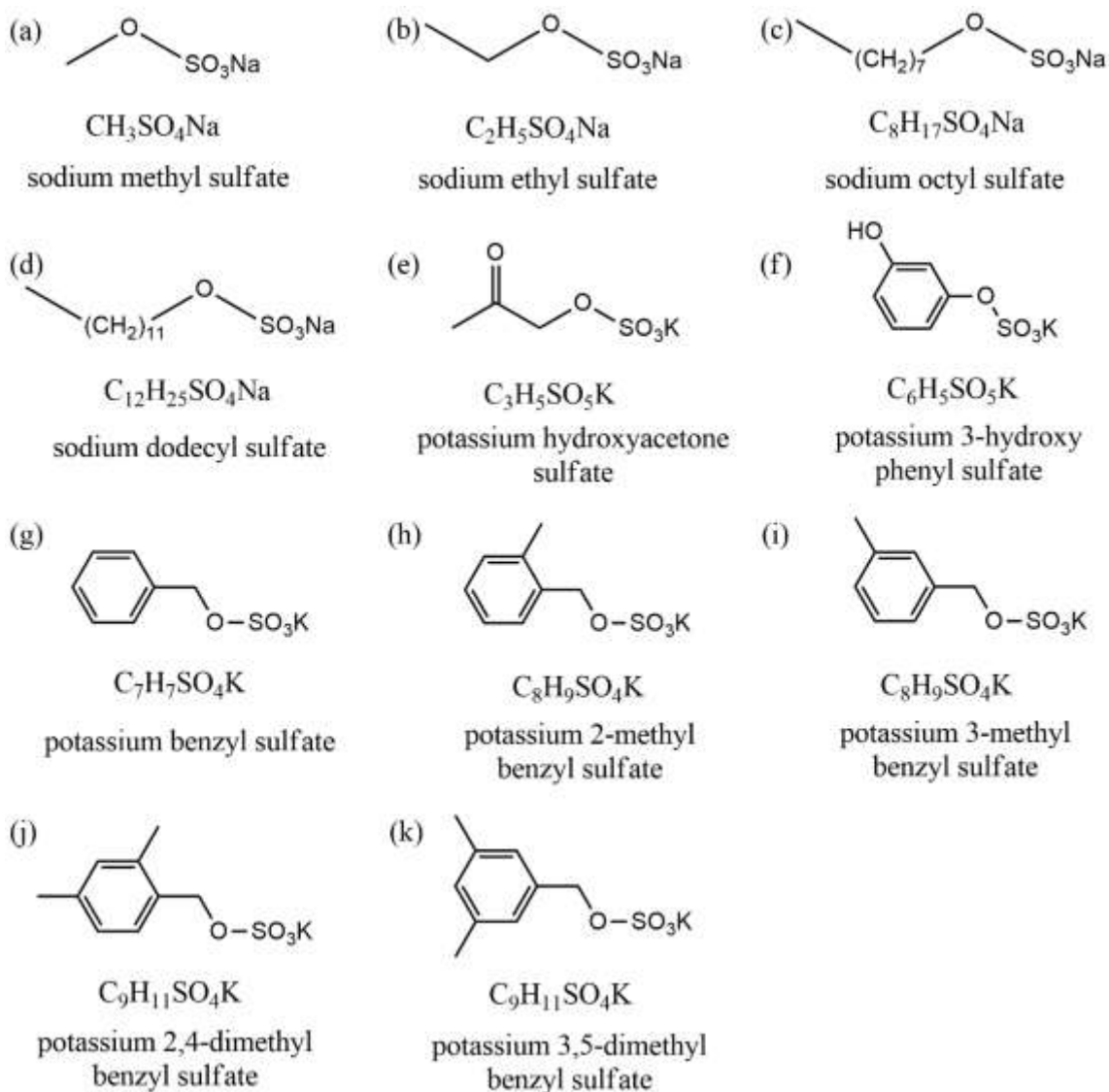
92 In this work, three complementary techniques were used to investigate hygroscopic properties  
93 and CCN activities of a series of OS, including sodium methyl sulfate, sodium ethyl sulfate,  
94 sodium octyl sulfate, sodium dodecyl sulfate, potassium hydroxyacetone sulfate, potassium 3-  
95 hydroxy phenyl sulfate, potassium benzyl sulfate, potassium 2-methyl benzyl sulfate, potassium  
96 3-methyl benzyl sulfate, potassium 2,4-dimethyl benzyl sulfate and potassium 3,5-dimethyl benzyl  
97 sulfate. A vapor sorption analyzer was employed to measure mass change of these OS samples as  
98 a function of RH. In addition, hygroscopic growth (change in mobility diameters) and CCN  
99 activation of submicron aerosol particles were studied for sodium methyl sulfate, sodium ethyl  
100 sulfate and sodium octyl sulfate, using a humidity tandem differential mobility analyzer (H-TDMA)  
101 and a cloud condensation nuclei counter (CCNc). Due to their very limited quantities, we could  
102 not carry out H-TDMA and CCNc measurements for other OS samples which were synthesized  
103 by us. In addition, we also investigated the impacts of sodium methyl sulfate, sodium ethyl sulfate  
104 and sodium octyl sulfate on hygroscopic properties and CCN activities of ammonium sulfate.

## 105 **2 Experimental section**

### 106 **2.1 Chemicals and reagents**

107 Sodium methyl sulfate ( $\text{CH}_3\text{SO}_4\text{Na}$ , >98%) and sodium ethyl sulfate ( $\text{C}_2\text{H}_5\text{SO}_4\text{Na}$ , >98%)  
108 were purchased from Tokyo Chemical Industry (TCI); sodium octyl sulfate ( $\text{C}_8\text{H}_{17}\text{SO}_4\text{Na}$ , >99%),  
109 sodium dodecyl sulfate ( $\text{C}_{12}\text{H}_{25}\text{SO}_4\text{Na}$ , >99%) and ammonium sulfate (>99.5%) were supplied by  
110 Aldrich. The other seven OS, including potassium hydroxyacetone sulfate, potassium 3-hydroxy  
111 phenyl sulfate, potassium benzyl sulfate, potassium 2-methyl benzyl sulfate, potassium 3-methyl  
112 benzyl sulfate, potassium 2,4-dimethyl benzyl sulfate and potassium 3,5-dimethyl benzyl sulfate,  
113 were synthesized using the method described by Huang et al. (2018), and their purities were found

114 to be >95% using nuclear magnetic resonance analysis. Chemical formulas and molecular  
115 structures of OS investigated in this study can be found in Figure 1.



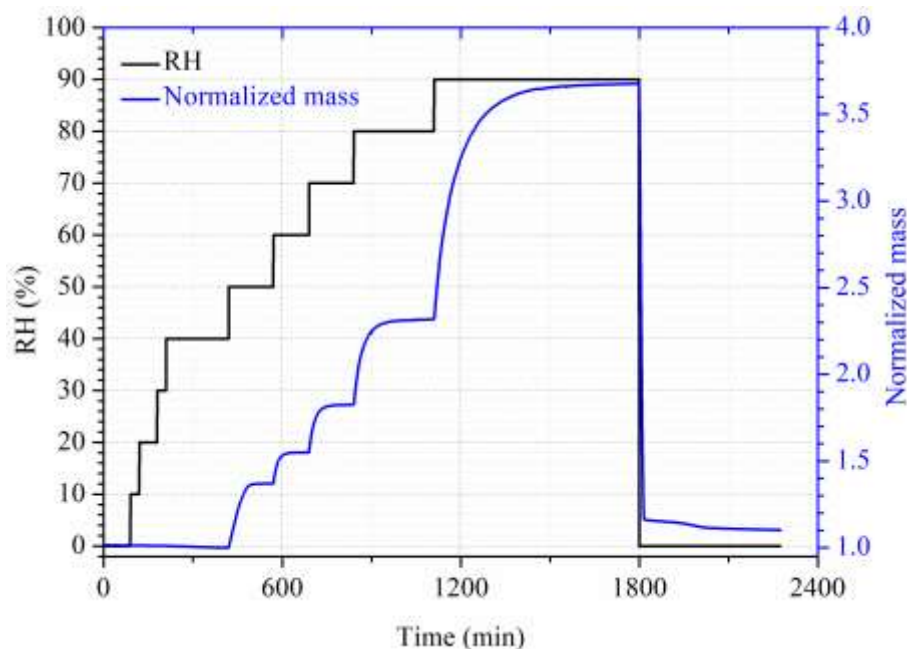
116  
117 **Figure 1.** Chemical formulas and molecular structures of organosulfates investigated in this study.

118

## 119 2.2 VSA experiments

120 A vapor sorption analyzer (VSA), commercialized by TA Instruments (New Castle, DE,  
121 USA), was used to measure mass change of organosulfates as a function of RH. Experimental

122 details can be found in our previous studies (Chen et al., 2019; Gu et al., 2017; Guo et al., 2019;  
123 Tang et al., 2019b), and are thus described here briefly. Experiments were conducted at  $25 \pm 0.1$  °C  
124 and in the RH range of 0-90%. A high precision balance was used to measure the sample mass at  
125 different RH with a stated sensitivity of  $<0.1$   $\mu\text{g}$ , and the dry mass of samples used in this work  
126 was typically around 1.0 mg.



127  
128 **Figure 2.** Change in RH (black curve, left y axis) and normalized sample mass (blue curve, right  
129 y axis) of  $\text{CH}_3\text{SO}_4\text{Na}$  with of time in a typical vapor sorption analyzer experiment at 25 °C.

130  
131 Changes in RH and normalized mass of a  $\text{CH}_3\text{SO}_4\text{Na}$  sample with time are displayed in Figure  
132 2 as an example to illustrate the VSA experimental procedure. As shown in Figure 2, the mass of  
133 OS samples at different RH was determined by the VSA using the following method. RH was set  
134 to  $<1\%$  to dry the sample; after the sample mass was stabilized, RH was increased to 90% stepwise  
135 with an interval of 10% per step; at the end, RH was changed back to  $<1\%$  to dry the sample again.  
136 The sample was considered to reach the equilibrium at a given RH when the mass change was

137 measured to be  $<0.1\%$  within 30 min. All the experiments were conducted at least three times in  
138 our work. The sample mass at a given RH ( $m$ ) was normalized to that at  $<1\%$  RH ( $m_0$ ) to determine  
139 the mass growth factor, defined as  $m/m_0$ .

### 140 **2.3 H-TDMA experiments**

141 A custom-built hygroscopicity tandem differential mobility analyzer (H-TDMA) was used to  
142 measure the mobility diameters of OS aerosol particles at different RH (5-90%) at  $24 \pm 1$  °C. The  
143 instrument was detailed elsewhere (Jing et al., 2016; Peng et al., 2016), and therefore only a brief  
144 introduction is given here. A commercial atomizer (MSP 1500) was used to produce polydisperse  
145 aerosol particles from dilute OS solutions in water (around 0.1 wt %), and the generated aerosol  
146 was dried to  $<5\%$  RH by passing the aerosol flow through a Nafion dryer (MD-110-12S) and then  
147 a silica gel diffusion dryer. The dry aerosol flow was subsequently split to two flows. One aerosol  
148 flow was sent to the vent, and the other aerosol flow ( $0.3 \text{ L min}^{-1}$ ) was passed through the first  
149 differential mobility analyzer (DMA) to produce quasi-monodisperse aerosol particles with a  
150 mobility diameter of 100 nm. After that, the aerosol flow was humidified to a desired RH by  
151 flowing through a humidification section, which was made of two Nafion tubes (MD-700-12F-1)  
152 connected in series, and the residence time in the humidification section was  $\sim 27$  s. Finally, the  
153 size distribution of humidified aerosol was measured by a scanning mobility particle sizer (SMPS),  
154 which consisted of the second DMA coupled to a condensation particle counter (CPC 3776, TSI).  
155 RH of the aerosol flow and the sheath flow in the second DMA were maintained to be equal and  
156 monitored using a commercial dew-point hygrometer (Michell, UK) with a stated uncertainty of  
157  $\pm 0.08\%$  RH. In addition, the flow rate ratio of the sheath flow to the aerosol flow was set to 10:1  
158 for both DMAs.

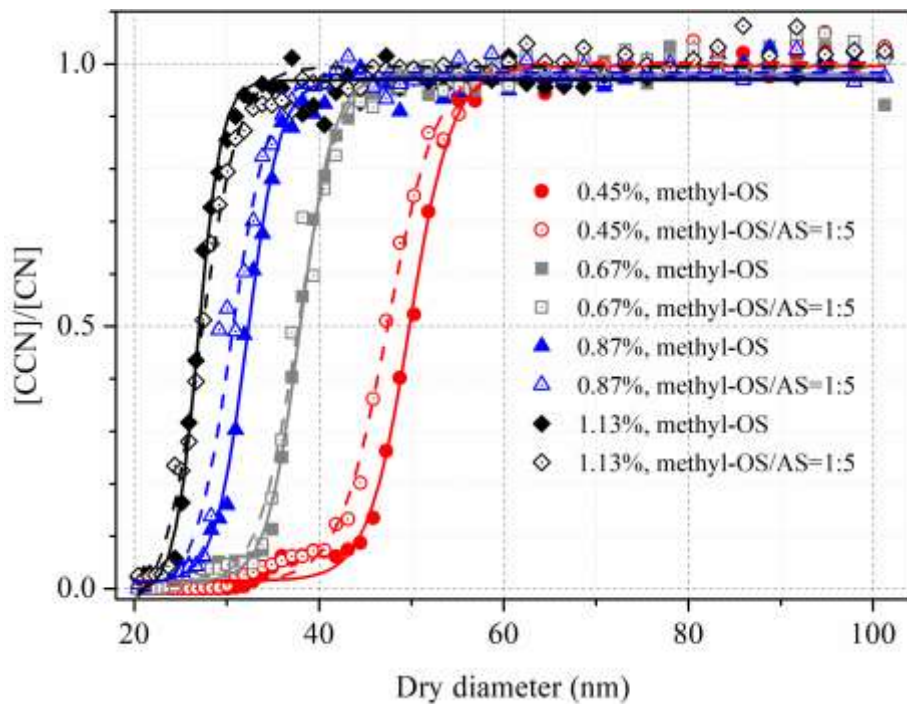
159 Hygroscopic growth factors (GF), defined as  $d/d_0$  ( $d$  is the mobility diameter at a given RH  
160 and  $d_0$  is the mobility diameter at RH <5%) were reported. All the experiments were conducted in  
161 triplicate. During our experiments, ammonium sulfate was used to calibrate the H-TDMA system  
162 routinely, and the absolute differences between the measured and theoretical GF at 90% RH were  
163 found to be within 0.04, confirming the robustness of our measurements.

#### 164 **2.4 CCN experiments**

165 The CCN activity of aerosol particles was determined using a commercial cloud condensation  
166 nuclei counter (CCNc, CCN-100, Droplet Measurement Technologies, Longmont, CO, USA)  
167 described in previous studies (Roberts and Nenes, 2005; Lance et al., 2006; Moore et al., 2010).  
168 Polydisperse aerosol particles were generated using a commercial atomizer (TSI 3076), in which  
169 concentrations of solutions used were around 0.1 g/L. The wet aerosol flow generated was passed  
170 through two silica gel diffusion dryers to reduce its RH to <5% RH. After that, a dry aerosol flow  
171 ( $\sim 800 \text{ mL min}^{-1}$ ) was passed through a DMA (TSI 3081) in size scanning mode to produce quasi-  
172 monodisperse aerosols, and subsequently the aerosol flow was split to two streams: one stream  
173 ( $\sim 300 \text{ mL/min}$ ) was sampled into a commercial CPC (TSI 3775) to measure total number  
174 concentrations of aerosol particles ([CN]), and the second flow ( $\sim 500 \text{ mL/min}$ ) was sampled into  
175 the cloud condensation nuclei counter (CCNc, CCN-100) to measure number concentrations of  
176 CCN ([CCN]).

177 Activation fractions ([CCN]/[CN]) of size-resolved dry particles were determined using the  
178 Scanning Mobility CCN Analysis (SMCA) method described elsewhere (Moore et al., 2010). In  
179 brief, the DMA was operated in the scanning voltage mode, and thus one activation curve  
180 (activation fractions as a function of dry diameter) could be obtained in 60-120s. The multiple  
181 charge effect was also corrected in this method, and in our work the supersaturation ( $SS$ ) was set

182 in the range of 0.45-1.13% with the stated uncertainty to be  $\pm 0.01\%$ . As shown in Figure 3,  
183 activation fractions of sodium methyl sulfate (methyl-OS) and its internally mixed aerosol with  
184 ammonium sulfate were measured at four different SS with dry mobility diameters between 20 and  
185 100 nm. Activation fractions were fitted versus dry diameters, and the critical particle diameter  
186 ( $d_{50}$ ) was determined as the dry diameter at which the activation fraction is equal to 0.5. During  
187 our measurements, ammonium sulfate was used to calibrate supersaturations, and the Pitzer-ion  
188 interaction model was applied in the calibration procedure to account for incomplete dissociation  
189 of ammonium sulfate at droplet activation (Pitzer and Mayorga, 1973; Clegg and Brimblecombe,  
190 1988). The corrected supersaturations were reported in our work.

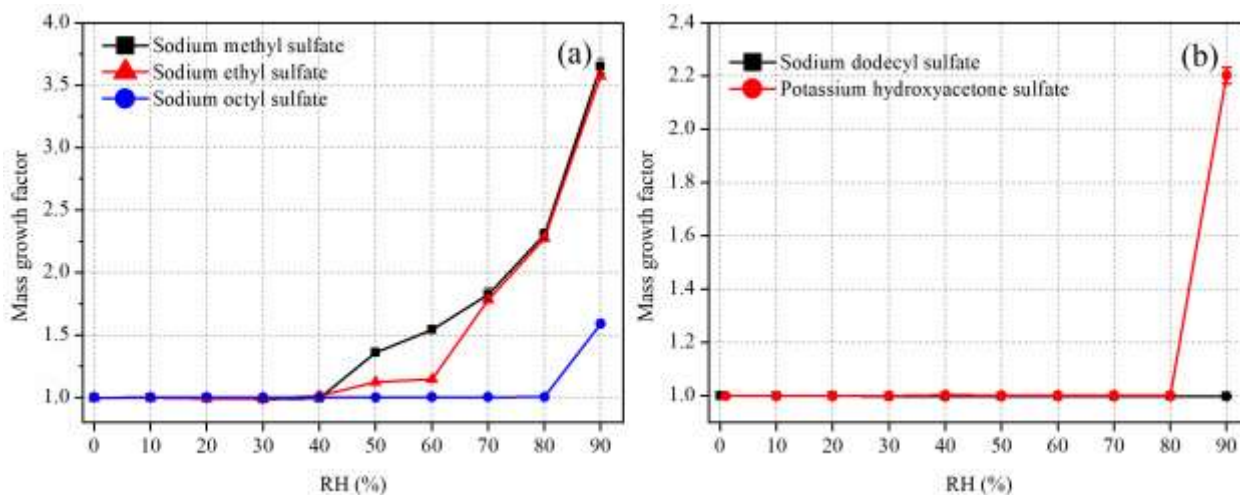


191  
192 **Figure 3.** Activation fractions of methyl-OS and its internally mixed aerosol particles with  
193 ammonium sulfate (AS) as a function of dry particle diameter at four supersaturations.  
194

### 195 3 Results and discussion

#### 196 3.1 Mass growth of organosulfates

197 Figure 4 displays mass growth factors of sodium methyl sulfate (methyl-OS), sodium ethyl  
198 sulfate (ethyl-OS), sodium octyl sulfate (octyl-OS), sodium dodecyl sulfate (dodecyl-OS) and  
199 potassium hydroxyacetone sulfate, and the data are also listed in Table 1. Figure 4a suggests that  
200 methyl-OS was deliquesced when RH was increased from 40% to 50%, and after that mass growth  
201 factors increased further with RH. The mass of ethyl-OS was moderately increased (by ~11%)  
202 when RH was increased from 40% to 50%, and further increase in RH to 60% led to additional  
203 while small increase in sample mass (by ~2%); the increase in sample mass at 50% and 60% RH  
204 may be because ethyl-OS were partially deliquesced at this stage (Ling and Chan, 2008; Mikhailov  
205 et al., 2009). When RH was increased to 70%, ethyl-OS was completely deliquesced, and further  
206 increase in RH (to 80% and 90%) resulted in further increase in sample mass. Octyl-OS was only  
207 deliquesced when RH was increased from 80% to 90%, whereas no significant water uptake was  
208 observed for dodecyl-OS even at 90% RH. The mass growth factors at 90% RH were determined  
209 to be  $3.65 \pm 0.06$ ,  $3.58 \pm 0.02$  and  $1.59 \pm 0.01$  for methyl-OS, ethyl-OS, and octyl-OS, respectively.



210

211 **Figure 4.** Mass growth factors of (a) methyl-, ethyl- and octyl-OS and (b) dodecyl-OS and  
212 potassium hydroxyacetone sulfate as a function of RH at 25 °C. Please note that error bars are  
213 included, but they are too small to be clearly visible.

214  
215 Mass growth factors of seven potassium organosulfates were also investigated, including  
216 potassium hydroxyacetone sulfate, potassium 3-hydroxy phenyl sulfate, potassium benzyl sulfate,  
217 potassium 2-methyl benzyl sulfate, potassium 3-methyl benzyl sulfate, potassium 2,4-dimethyl  
218 benzyl sulfate and potassium 3,5-dimethyl benzyl sulfate. All the compounds did not show  
219 measurable water uptake at 80% RH. When RH was increased to 90%, as shown in Figure 4b, a  
220 significant increase in mass was observed for potassium hydroxyacetone sulfate particles,  
221 suggesting the occurrence of deliquescence, and the mass growth factor was determined to be  
222  $2.20 \pm 0.03$  at 90% RH. Furthermore, no significant water uptake was observed for the other six  
223 potassium organosulfates even when RH was increased to 90%. We should mention that  
224 occasionally small increase in sample mass (up to 10-20%) was observed for a few samples when  
225 RH was increased from 80% to 90%, and such small increase in sample mass may be caused by  
226 water uptake of impurities (such as potassium hydroxide) contained in these synthesized  
227 compounds. When such increase sample mass was observed when RH was increased from 80% to  
228 90%, we carried out at least four duplicate experiments, and all the other experiments confirmed  
229 that mass increase was insignificant.

230  
231 **Table 1.** Mass growth factors ( $m/m_0$ ) and water-to-solute ratios (WSRs) as a function of RH (10-  
232 90 %) at 25 °C for sodium methyl sulfate, sodium ethyl sulfate, sodium octyl sulfate and potassium  
233 hydroxyacetone sulfate. All the errors given in this work are standard deviations.

RH (%)	sodium methyl sulfate		sodium ethyl sulfate	
	$m/m_0$	WSR	$m/m_0$	WSR
10	1.00±0.01	-	1.00±0.01	-
20	1.00±0.01	-	0.99±0.01	-
30	0.99±0.01	-	0.99±0.01	-
40	1.00±0.02	-	1.02±0.03	-
50	1.36±0.02	2.68±0.04	1.13±0.01	-
60	1.55±0.03	4.06±0.09	1.15±0.01	-
70	1.83±0.05	6.16±0.17	1.79±0.02	6.46±0.07
80	2.31±0.04	9.73±0.18	2.27±0.02	10.48±0.11
90	3.65±0.06	19.75±0.34	3.58±0.02	21.19±0.14

RH (%)	sodium octyl sulfate		potassium hydroxyacetone sulfate	
	$m/m_0$	WSR	$m/m_0$	WSR
10	1.00±0.01	-	1.00±0.01	-
20	1.00±0.01	-	1.00±0.01	-
30	1.00±0.01	-	1.00±0.01	-
40	1.00±0.01	-	1.00±0.01	-
50	1.00±0.01	-	1.00±0.01	-
60	1.00±0.01	-	1.00±0.01	-
70	1.00±0.01	-	1.00±0.01	-
80	1.01±0.01	-	1.00±0.01	-
90	1.59±0.01	7.63±0.02	2.20±0.03	12.84±0.18

234

235 For deliquesced samples, measured mass changes can be converted to water to solute ratios

236 (WSRs), defined as the molar ratio of H<sub>2</sub>O to sulfur. The WSRs data are summarized in Table 1

237 for sodium methyl sulfate, sodium ethyl sulfate, sodium octyl sulfate and potassium

238 hydroxyacetone sulfate. As shown in Table 1, WSRs at 90% RH were determined to be 19.75±0.34,

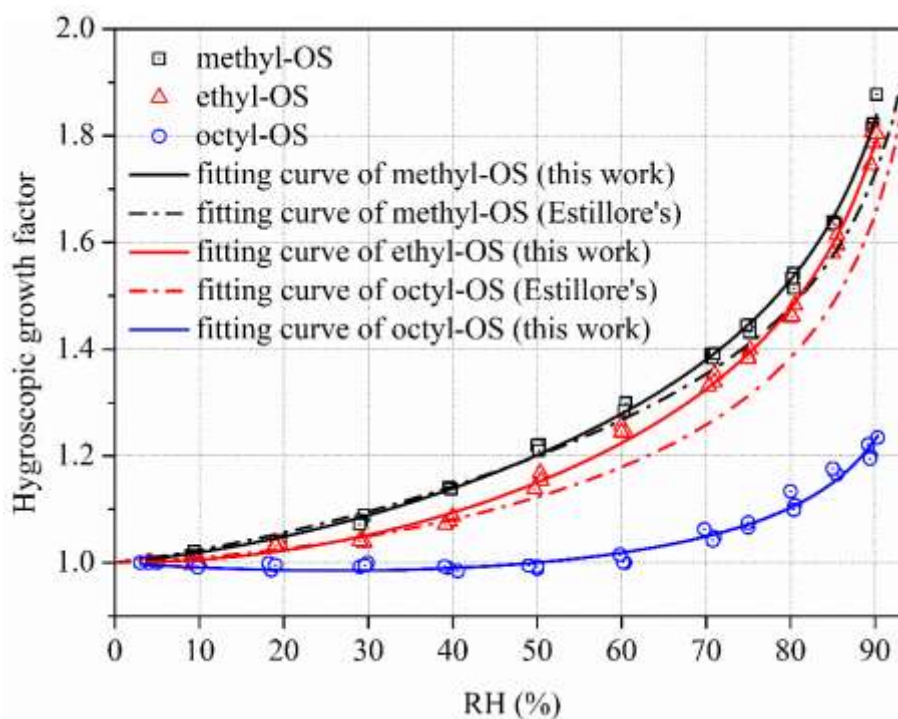
239 21.19±0.14, 7.63±0.02 and 12.84±0.18 for sodium methyl sulfate, sodium ethyl sulfate, sodium

240 octyl sulfate and potassium hydroxyacetone sulfate at 25 °C.

## 241 3.2 Hygroscopic growth of aerosols

### 242 3.2.1 Organosulfates

243 H-TDMA was employed to measure hygroscopic growth factors of 100 nm methyl-, ethyl-  
244 and octyl-OS aerosols as a function of RH (up to 90%), and the results are shown in Figure 5 and  
245 Table 2. In addition, no significant hygroscopic growth was observed for dodecyl-OS for RH up  
246 to 90%. We did not investigate hygroscopic growth of other OS aerosols due to the very small  
247 quantity of these synthesized compounds.



248  
249 **Figure 5.** Hygroscopic growth factors of (a) methyl- and octyl-OS and (b) ethyl-OS aerosols as a  
250 function of RH. Solid curves represent fitted curves in our work using Eq. (1). For comparison,  
251 the fitted curves reported by Estillore et al. (2016) are presented by dashed curves.

252  
253 As shown in Figure 5, methyl-, ethyl- and octyl-OS aerosols all exhibited continuous  
254 hygroscopic growth without obvious phase transitions. To our knowledge, only one previous study

255 (Estillore et al., 2016) investigated hygroscopic growth of methyl- and ethyl-OS aerosols using a  
 256 H-TDMA, and continuous hygroscopic growth was also observed. The continuous growth  
 257 behavior can be attributed to the amorphous state of aerosol particles, which would take up water  
 258 at very low RH. For methyl-OS aerosol, GFs were determined in our work to be  $1.53 \pm 0.01$ ,  
 259  $1.63 \pm 0.01$  and  $1.83 \pm 0.03$  at 80%, 85% and 90% RH; for comparison, its GF was measured to be  
 260 1.50 at 85% RH by Estillore et al. (2016), only ~8% smaller than our result. In our work, GFs were  
 261 determined to be  $1.47 \pm 0.01$ ,  $1.60 \pm 0.02$  and  $1.79 \pm 0.02$  at 80%, 85% and 90% RH for ethyl-OS  
 262 aerosol; for comparison, it was measured to be 1.45 at 85% RH in the previous study (Estillore et  
 263 al., 2016), only ~9% smaller than our result. As DMA sizing typically has a relative uncertainty of  
 264 5-7% (Wiedensohler et al., 2012), our measured GFs agree very well with those reported by  
 265 Estillore et al. (2016) for methyl- and ethyl-OS, while the highest RH we reached was 90%,  
 266 compared to 85% by Estillore et al. (2016). With respect to octyl-OS aerosol, GF were determined  
 267 to be  $1.11 \pm 0.02$ ,  $1.17 \pm 0.01$  and  $1.21 \pm 0.02$  at 80%, 85% and 90% RH in our work; to our knowledge,  
 268 hygroscopic growth of octyl-OS aerosol has not been explored previously. Compared to  
 269 ammonium sulfate (1.75 at 90% RH), GFs at 90% RHs were found to be slightly larger for methyl-  
 270 and ethyl-OS, but significantly smaller for octyl-OS.

271

272 **Table 2.** Hygroscopic growth factors (GFs) of methyl-, ethyl- and octyl-OS aerosols at different  
 273 RH. All the errors given in this work are standard deviations.

RH (%)	sodium methyl sulfate	sodium ethyl sulfate	sodium octyl sulfate
5	$1.00 \pm 0.01$	$1.00 \pm 0.01$	$1.00 \pm 0.01$
10	$1.01 \pm 0.01$	$1.00 \pm 0.01$	$1.00 \pm 0.01$
20	$1.04 \pm 0.01$	$1.03 \pm 0.01$	$0.99 \pm 0.01$
30	$1.08 \pm 0.01$	$1.04 \pm 0.01$	$1.00 \pm 0.01$

40	1.14±0.01	1.08±0.01	0.99±0.01
50	1.22±0.01	1.15±0.01	0.99±0.01
60	1.29±0.01	1.25±0.01	1.01±0.01
70	1.39±0.01	1.34±0.01	1.05±0.01
75	1.44±0.01	1.39±0.01	1.07±0.01
80	1.53±0.01	1.47±0.01	1.11±0.02
85	1.63±0.01	1.60±0.02	1.17±0.01
90	1.83±0.03	1.79±0.02	1.21±0.02

274

275 When aerosol particles take up water continuously, the RH-dependent GFs can usually be  
 276 fitted using Eq. (1) (Kreidenweis et al., 2005):

$$277 \quad GF = [1 + (a + b \cdot \frac{RH}{100} + c \cdot (\frac{RH}{100})^2) \cdot \frac{RH}{100 - RH}]^{1/3} \quad (1)$$

278 where  $a$ ,  $b$  and  $c$  are coefficients obtained from fitting using Eq. (1). As shown in Figure 5,  
 279 hygroscopic growth factors of methyl-, ethyl- and octyl-OS aerosols can be fitted by Eq. (1), and  
 280 the obtained coefficients ( $a$ ,  $b$  and  $c$ ) are summarized in Table 3.

281

282 **Table 3.** The three coefficients ( $a$ ,  $b$  and  $c$ ) obtained by using Eq. (1) to fit RH-dependent GFs for  
 283 sodium methyl sulfate, sodium ethyl sulfate and sodium octyl sulfate aerosols.

organosulfates	$a$	$b$	$c$
sodium methyl sulfate	0.42182	1.20336	-1.15508
sodium ethyl sulfate	0.00174	1.61805	-1.15502
sodium octyl sulfate	-0.31868	0.86233	-0.44623

284

### 285 3.2.2 Comparison between VSA and H-TDMA measurements

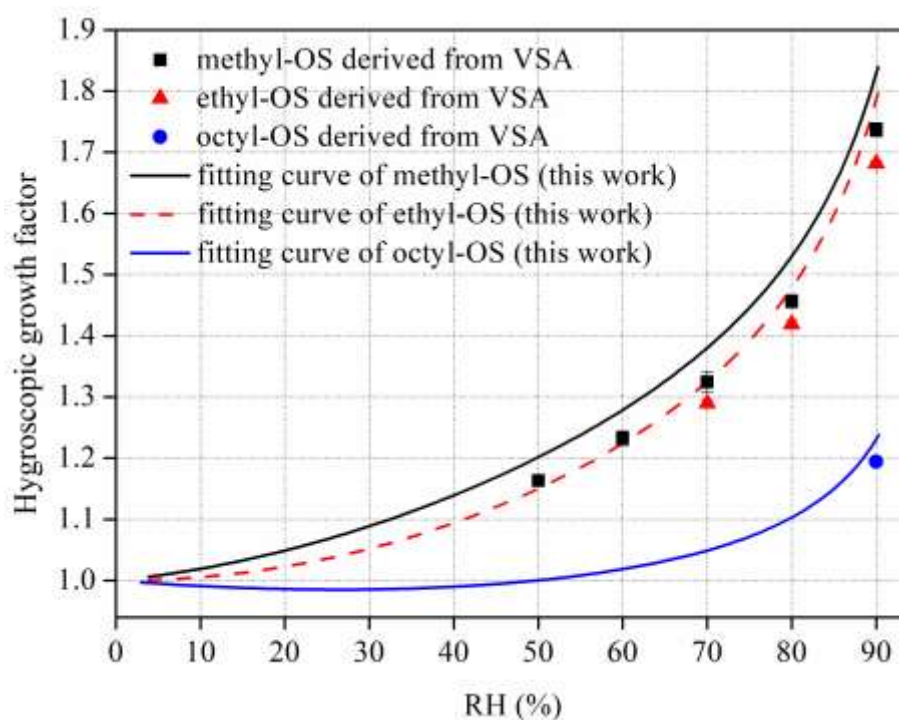
286 Figure 4 shows that obvious deliquescence transitions were observed for methyl-, ethyl-, and  
287 octyl-OS in the VSA experiments, because samples used in VSA experiments may be crystalline  
288 salts; in contrast, as revealed by Figure 5, continuous hygroscopic growth without obvious phase  
289 transitions was observed for methyl-, ethyl- and octyl-OS aerosol particles in H-TDMA  
290 measurements, suggesting that these aerosol particles which were produced by drying aqueous  
291 droplets to <5% RH may exist in amorphous state. Estillore et al. (2016) employed a H-TDMA to  
292 investigate hygroscopic properties of several OS aerosols, and similarly they found that those  
293 aerosols, including methyl-OS, ethyl-OS and potassium hydroxyacetone sulfate which were also  
294 examined in our work, displayed continuous hygroscopic growth.

295 For completely deliquesced particles, if it is assumed that the particle is spherical and that the  
296 particle volume at a given RH is equal to the sum of the dry particle volume and the volume of  
297 particulate water, particle mass change, measured using the VSA, can then be converted to  
298 hygroscopic GF, using Eq. (2):

$$299 \quad GF = \sqrt[3]{1 + \left(\frac{m}{m_0} - 1\right) \cdot \frac{\rho_0}{\rho_w}} \quad (2)$$

300 where  $\rho_0$  and  $\rho_w$  are the density of the dry sample and water, respectively. The density of methyl-,  
301 ethyl- and octyl-OS particles were reported to be 1.60, 1.46 and 1.19 g cm<sup>-3</sup> with an uncertainty of  
302 20-30% (Kwong et al., 2018; ChemistryDashboard, 2021). Figure 6 compares VSA-derived GFs  
303 and those measured using H-TDMA for methyl-, ethyl- and octyl-OS, and it can be concluded that  
304 for RH at which samples used in the VSA experiments were deliquesced, GFs derived from mass  
305 change measured using VSA agree relatively well with those directly measured using H-TDMA.  
306 For example, at 90% RH GFs were measured by H-TDMA to be 1.83±0.03, 1.79±0.02 and  
307 1.21±0.02 for methyl-, ethyl- and octyl-OS, while at the same RH their GFs derived from VSA

308 measurements were found to be  $1.74 \pm 0.01$ ,  $1.68 \pm 0.01$  and  $1.19 \pm 0.01$ , only 6% (or less) smaller  
309 than those measured using H-TDMA. The small but systematic differences between VSA and  
310 H-TDMA results, as evident from Figure 6, could stem from volume additivity assumption used  
311 to convert mass growth to diameter growth, uncertainties in OS densities, and DMA sizing errors.



312  
313 **Figure 6.** Comparison between hygroscopic GFs of methyl-, ethyl- and octyl-OS derived from  
314 VSA experiments to those measured using H-TDMA. Please note that H-TDMA results are  
315 presented as the three-parameter curves obtained. Error bars are included, but they are too small  
316 to be clearly visible.

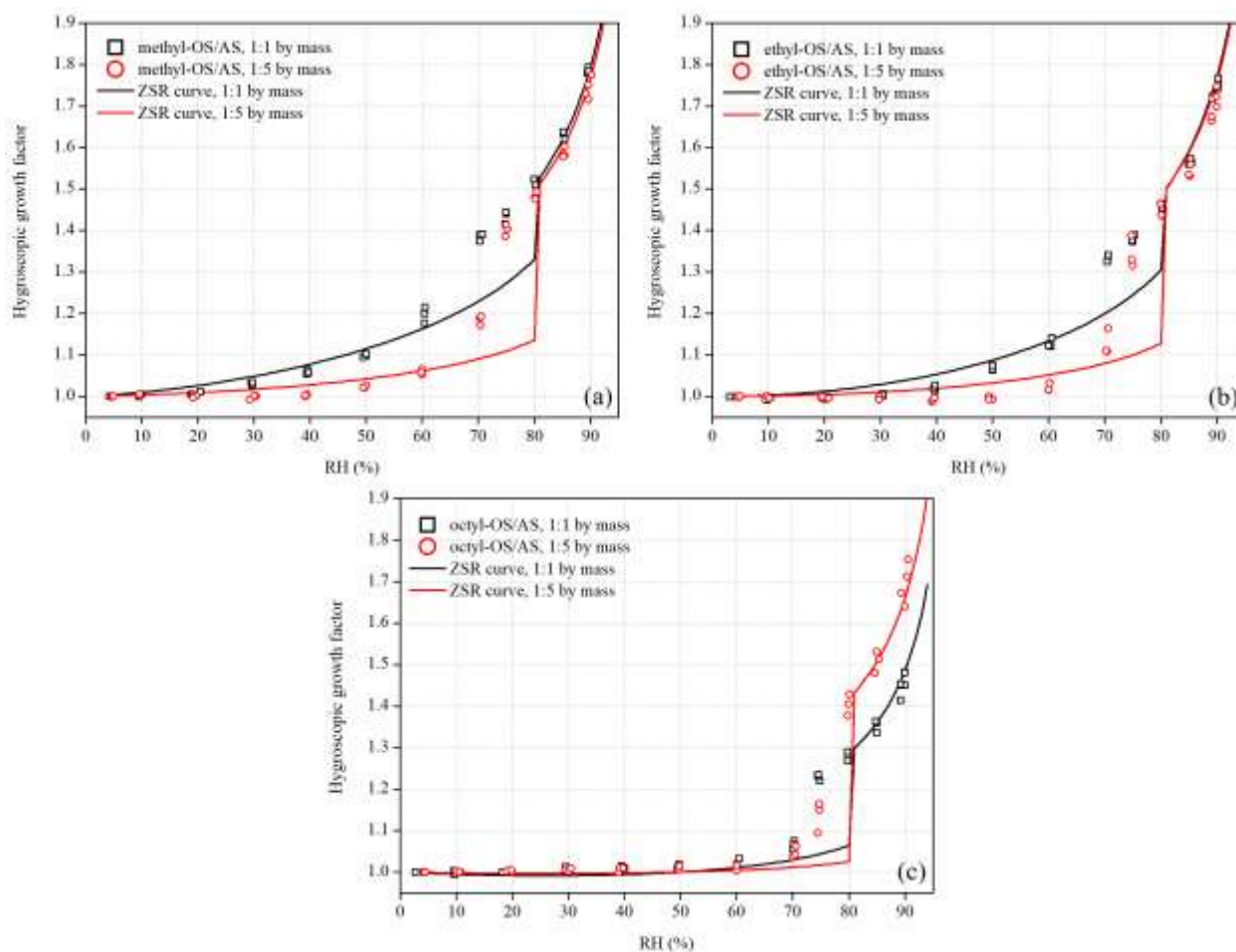
317

### 318 3.2.3 Internally mixed aerosols

319 We also investigated hygroscopic properties of methyl-, ethyl- and octyl-OS aerosols  
320 internally mixed with ammonium sulfate (AS), and the results are summarized in Table 4. Figure  
321 7a displays GFs of 100 nm methyl-OS/AS mixed aerosols with mass ratios of 1:1 and 1:5. The 1:1

322 mixed aerosol particle showed a deliquescence transition at 70% RH, while the 1:5 mixed aerosols  
323 showed a deliquescence transition at 75% RH, which was lower than the deliquescence RH (DRH,  
324 80%) of AS. Here the DRH is defined as the RH at which the mixed aerosols are completely  
325 deliquesced (Choi and Chan, 2002). Figure 7a suggests that before full deliquescence, significant  
326 hygroscopic growth was also observed, i.e. pre-deliqescence of mixed particles occurred when  
327 RH was lower than their DRH. Pre-deliqescence was widely reported in previous studies which  
328 investigated hygroscopic properties of inorganic/organic mixed aerosols (Choi and Chan, 2002;  
329 Prenni, 2003; Wise et al., 2003; Brooks, 2004; Marcolli and Krieger, 2006; Wu et al., 2011; Lei et  
330 al., 2014; Jing et al., 2016; Estillore et al., 2017). For example, Choi and Chan. (2002) investigated  
331 hygroscopic behaviors of internal mixed particles which consisted of water-soluble organic  
332 compounds and AS, and found that the internal mixing with organics (such as malonic and citric  
333 acids) could reduce the DRH of AS, due to the ability of organics to absorb water at low RH.

334 Internal mixing with ethyl- and octyl-OS could also reduce the DRH of AS. As shown in  
335 Figure 7b, ethyl-OS/AS mixed aerosols were deliquesced at 70% RH when the mass ratio of ethyl-  
336 OS to AS was 1:1 and at 80% RH when the mass ratio was 1:5. In addition, Figure 7c suggested  
337 that the deliquescence of octyl-OS/AS aerosols took place at 75% RH for the 1:1 mixture and at  
338 80% for 1:5 mixture.



339  
 340 **Figure 7.** Hygroscopic growth factors of (a) methyl-OS/AS, (b) ethyl-OS/AS, and (c) octyl-OS/AS  
 341 aerosols as a function of RH. The mass ratios of methyl-, ethyl-, and octyl-OS to AS were 1:1 and  
 342 1:5, respectively. Solid curves represent hygroscopic growth factors of mixed aerosols predicted  
 343 using the ZSR method.

344  
 345 **Table 4.** Hygroscopic GF of methyl-, ethyl, and octyl-OS internally mixed with AS (their mass  
 346 ratios are 1:1 and 1:5) at different RH. All the errors given in this work are standard deviations.

RH (%)	methyl-OS/AS		ethyl-OS/AS		octyl-OS/AS	
	1:1	1:5	1:1	1:5	1:1	1:5
5	1.00±0.01	1.00±0.01	1.00±0.01	1.00±0.01	1.00±0.01	1.00±0.01
10	1.00±0.01	1.00±0.01	1.00±0.01	1.00±0.01	1.00±0.01	1.00±0.01

20	1.01±0.01	1.00±0.01	1.00±0.01	1.00±0.01	1.00±0.01	1.00±0.01
30	1.03±0.01	1.00±0.01	1.00±0.01	1.00±0.01	1.01±0.01	1.01±0.01
40	1.06±0.01	1.00±0.01	1.02±0.01	0.99±0.01	1.01±0.01	1.01±0.01
50	1.10±0.01	1.02±0.01	1.07±0.01	0.99±0.01	1.01±0.01	1.01±0.01
60	1.20±0.02	1.06±0.01	1.13±0.01	1.02±0.01	1.02±0.01	1.01±0.01
70	1.38±0.01	1.19±0.01	1.33±0.01	1.13±0.03	1.07±0.01	1.05±0.01
75	1.43±0.01	1.40±0.01	1.38±0.01	1.34±0.04	1.23±0.01	1.14±0.03
80	1.52±0.01	1.48±0.01	1.46±0.01	1.45±0.02	1.28±0.01	1.40±0.02
85	1.63±0.01	1.59±0.01	1.56±0.01	1.54±0.02	1.35±0.02	1.51±0.02
90	1.79±0.01	1.74±0.02	1.74±0.02	1.72±0.02	1.47±0.02	1.69±0.04

347

348 The Zdanovskii-Stokes-Robinson (ZSR) method (Stokes and Robinson, 1966) has been  
349 widely used to predict hygroscopic growth of internally mixed aerosol particles, assuming that the  
350 interaction among individual species are negligible and that individual species in the mixed  
351 particles take up water independently. According to the ZSR method, GF of a mixed particle,  $GF_{\text{mix}}$ ,  
352 can be calculated using Eq. (3) (Malm and Kreidenweis, 1997):

$$353 \quad GF_{\text{mix}} = \sqrt[3]{\sum(\varepsilon_i \cdot GF_i^3)} \quad (3)$$

354 where  $GF_i$  is the GF of  $i$ th species the dry mixed particle contains. The volume fraction of the  $i$ th  
355 species in the dry mixed particle,  $\varepsilon_i$ , can be calculated using Eq. (4):

$$356 \quad \varepsilon_i = \frac{m_i/\rho_i}{\sum(m_i/\rho_i)} \quad (4)$$

357 where  $m_i$  and  $\rho_i$  are the mass fraction and density of the  $i$ th species. GFs of pure OS, measured in  
358 our work using H-TDMA and presented in Section 3.2.1, and GFs of AS, calculated using the E-  
359 AIM model (Clegg et al., 1998; Wexler and Clegg, 2002), were used as input to predict GFs of  
360 methyl-, ethyl- and octyl-OS internally mixed with AS. Comparisons between measured and  
361 predicted GFs are displayed in Figure 7 for OS/AS mixed aerosols.

362 As shown in Figure 7a, GFs of methyl-OS/AS mixed aerosols (both the 1:1 and 1:5 mixtures)  
 363 could be well predicted using the ZSR method when RH was <60% or >80%, while the ZSR  
 364 method underestimated their GFs at 70% and 75% RH. Such underestimation at 70% and 75% RH  
 365 is likely to due to that inorganic compounds (AS, in our work) may dissolve partially in the  
 366 organics/water solution (which can be formed at much lower RH due to continuous water uptake  
 367 of organics) before the mixed particle is completely deliquesced (Svenningsson et al., 2006;  
 368 Zardini et al., 2008; Wu et al., 2011); in contrast, the ZSR method assumes that individual species  
 369 take up water independently. As shown in Figure 7, the ZSR method also underestimated GFs at  
 370 70 and 75% RH for ethyl-OS/AS and octyl-OS/AS mixed aerosols, though good agreement  
 371 between measurement and prediction was found at other RH. For example, the ratios of partially  
 372 dissolved AS to total AS at 70% RH were estimated to be 0.95, 0.85 and 0.49 for methyl-OS/AS,  
 373 ethyl-OS/AS, and octyl-OS/AS mixtures with a mass ratio of 1:1.

### 374 **3.3 Cloud condensation nucleation activities**

375 Figures 3, S2 and S3 show CCN activation curves obtained at four supersaturations for  
 376 methyl-, ethyl- and octyl-OS aerosols and their internal mixtures with ammonium sulfate. Each  
 377 activation curve was fitted using a Boltzmann sigmoid function to derive the corresponding critical  
 378 particle diameter ( $d_{50}$ ), which was then used to calculate  $\kappa_{ccn}$  using Eqs. (5a-5b) (Petters and  
 379 Kreidenweis, 2007):

$$380 \quad \kappa_{ccn} = \frac{4A^3}{27d_{50}^3 \ln^2 S_c} \quad (5a)$$

$$381 \quad A = \frac{4\sigma_{s/a}M_w}{RT\rho_w} \quad (5b)$$

382 where  $S_c$  is the critical saturation ratio ( $1+SS$ ) of water;  $d_{50}$  is the critical particle diameter;  $A$  is a  
 383 constant which describes the Kelvin effect on a curved surface of a droplet, and depends on the  
 384 surface tension ( $\sigma_{s/a}$ ), molecular weight ( $M_w$ ), density ( $\rho_w$ ) of water, temperature ( $T$ ) and the

385 universal gas constant ( $R$ ). Table 5 summarizes critical diameters at different supersaturations for  
 386 aerosol particles examined in this work and their  $\kappa_{\text{ccn}}$  values.

387

388 **Table 5.** Single hygroscopicity parameters derived from hygroscopic growth ( $\kappa_{\text{gf}}$ ) and CCN  
 389 activity measurements ( $\kappa_{\text{ccn}}$ ) for methyl-, ethyl- and octyl-OS and their internal mixtures with  
 390 ammonium sulfate (AS). All errors given were standard deviations.

aerosol	mass ratio	SS (%)	$d_{50}$ (nm)	$\kappa_{\text{ccn}}$	average $\kappa_{\text{ccn}}$	$\kappa_{\text{gf}}$
methyl-OS	-	0.45	52.9±0.9	0.432-0.477	0.459±0.021	0.537-0.604
	-	0.67	41.1±0.8	0.416-0.468		
	-	0.87	33.3±0.4	0.471-0.507		
	-	1.13	28.8±0.5	0.431-0.477		
methyl-OS/AS	1:5	0.45	51.9±0.5	0.467-0.492	0.453±0.027	0.454-0.495
	1:5	0.67	41.6±0.4	0.411-0.436		
	1:5	0.87	33.7±0.5	0.453-0.490		
	1:5	1.13	29.2±0.6	0.412-0.464		
ethyl-OS	-	0.45	55.5±0.8	0.375-0.410	0.397±0.010	0.505-0.548
	-	0.67	42.8±0.6	0.376-0.406		
	-	0.87	35.3±0.5	0.395-0.428		
	-	1.13	30.2±0.3	0.382-0.408		
ethyl-OS/AS	1:5	0.45	52.3±1.2	0.437-0.504	0.458±0.024	0.435-0.474
	1:5	0.67	41.0±0.5	0.426-0.459		
	1:5	0.87	33.4±0.6	0.463-0.512		
	1:5	1.13	29.2±0.6	0.409-0.462		
octyl-OS	-	0.45	70.0±1.2	0.186-0.207	0.206±0.008	0.076-0.096
	-	0.67	53.2±0.6	0.196-0.211		
	-	0.87	44.1±0.7	0.202-0.221		
	-	1.13	37.1±0.8	0.200-0.227		
octyl-OS/AS	1:5	0.45	53.7±0.9	0.413-0.456	0.436±0.009	0.388-0.464
	1:5	0.67	41.1±0.5	0.426-0.458		
	1:5	0.87	34.4±0.5	0.427-0.462		

391

392

393

394

395

396

397

398

399

As shown in Table 5,  $\kappa_{\text{ccn}}$  values were determined to be  $0.459 \pm 0.021$ ,  $0.397 \pm 0.010$  and  $0.206 \pm 0.008$  for methyl-, ethyl- and octyl-OS, decreasing with alkyl chain length, and this suggests that the addition of hydrophobic hydrocarbon functional groups to OS reduced their hygroscopicity. Decrease in hygroscopicity of OS compounds with the increase in the number of carbon atoms was also observed under subsaturated conditions (Section 3.2). In addition, we investigated CCN activities of alkyl-OS/AS mixed aerosols with a mass ratio of 1:5, and  $\kappa_{\text{ccn}}$  values were determined to be  $0.453 \pm 0.027$ ,  $0.458 \pm 0.024$  and  $0.436 \pm 0.009$  for methyl-OS/AS, ethyl-OS/AS and octyl-OS/AS.

400

### 3.3.1 Comparison between H-TDMA and CCN activities measurements

401

402

403

404

405

It is suggested that the single hygroscopicity parameter,  $\kappa$ , could describe aerosol-water interactions under both sub- and supersaturated conditions (Petters and Kreidenweis, 2007). The  $\kappa$  values derived from CCN activity measurements,  $\kappa_{\text{ccn}}$ , have been illustrated above; the  $\kappa$  values derived from H-TDMA measurements,  $\kappa_{\text{gf}}$ , can be calculated using Eq. (6) (Petters and Kreidenweis, 2007; Tang et al., 2016):

406

$$\kappa_{\text{gf}} = (\text{GF}^3 - 1) \frac{1 - \text{RH}}{\text{RH}} \quad (6)$$

407

408

409

In this work GF measured at 90% RH were used to calculate  $\kappa_{\text{gf}}$  values, which are also listed in Table 5. Eq. (6) does not take into account the Kelvin effect as the effect is small for 100 nm particles (Tang et al., 2016).

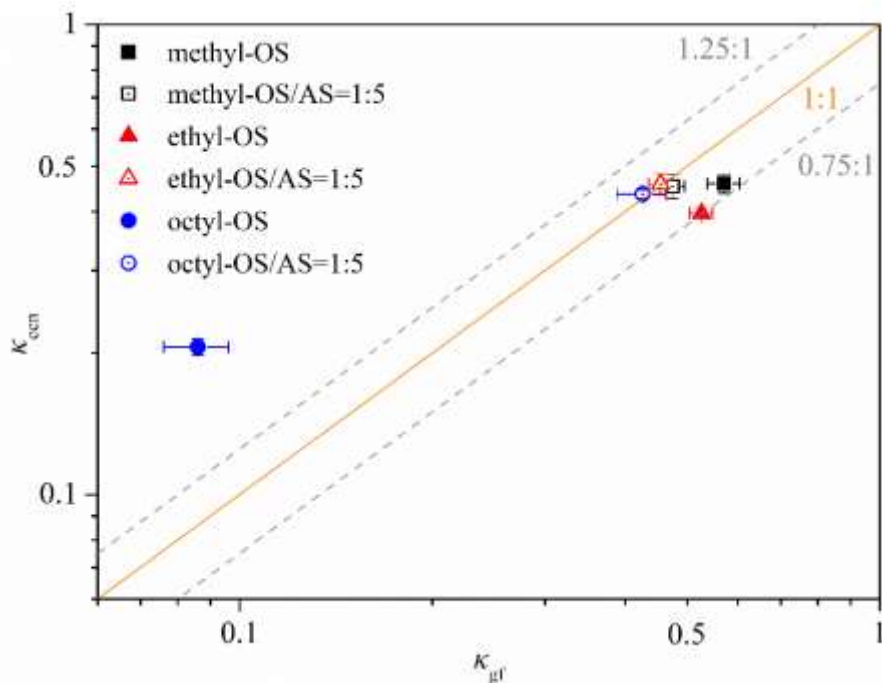
410

411

412

Figure 8 compares  $\kappa_{\text{ccn}}$  and  $\kappa_{\text{gf}}$  values for the six types of aerosol particles examined. For pure OS,  $\kappa_{\text{ccn}}$  of methyl-OS ( $0.459 \pm 0.021$ ) and ethyl-OS ( $0.397 \pm 0.010$ ) were smaller than their  $\kappa_{\text{gf}}$  values (0.537-0.604 and 0.505-0.548), but the relative differences do not exceed 25%. Such a

413 difference (<25%) may not be significant if all the uncertainties associated with deriving  $\kappa$  from  
 414 measured hygroscopic growth and CCN activities (Petters and Kreidenweis, 2007). Octyl-OS  
 415 appears to be an exception, and the average  $\kappa_{\text{ccn}}$  (0.206) was  $\sim 2.4$  times larger than the average  $\kappa_{\text{gf}}$   
 416 (0.086). In addition, no significant difference was observed between  $\kappa_{\text{ccn}}$  and  $\kappa_{\text{gf}}$  for all the alkyl-  
 417 OS/AS mixed aerosols.



418  
 419 **Figure 8.** Comparison of  $\kappa$  values derived from hygroscopic growth ( $\kappa_{\text{gf}}$ ) with these derived from  
 420 CCN activities ( $\kappa_{\text{ccn}}$ ) for methyl-, ethyl- and octyl-OS aerosols as well as their internal mixtures  
 421 with ammonium sulfate (the mass ratio was 1:5).

422  
 423 Significant differences between  $\kappa_{\text{gf}}$  and  $\kappa_{\text{ccn}}$  were reported in previous studies (Petters et al.,  
 424 2009; Wex et al., 2009; Hansen et al., 2015), attributed to several factors discussed below. Petters  
 425 and Kreidenweis. (2008) demonstrated that cloud droplet activation was highly sensitive to the  
 426 solubility for sparingly soluble compounds in the range of  $5 \times 10^{-4}$ - $2 \times 10^{-1}$ , expressed as volume of

427 solute per unit volume of water (Petters and Kreidenweis, 2008). Compared to the highly soluble  
428 methyl- and ethyl-OS (their solubilities are 0.127-0.219 and 0.075-0.151), the solubility of octyl-  
429 OS ( $8.43 \times 10^{-4}$ - $4.26 \times 10^{-2}$ ) (Chemistry Dashboard, 2021) is rather limited, and incomplete  
430 dissolution at subsaturated condition in H-TDMA measurements may lead to underestimation of  
431  $\kappa_{gf}$  values for octyl-OS; as a result, the solubility limit may explain the observed difference between  
432  $\kappa_{gf}$  and  $\kappa_{ccn}$  for octyl-OS. Furthermore, surface tension is a key factor to influence critical  
433 supersaturations at which aerosol particles are activated to cloud droplets (Petters and Kreidenweis,  
434 2013). We measured surface tensions of alkyl-OS and alkyl-OS/AS (the mass ratio was 1:5)  
435 solutions, and the results are shown in Table S1 and Figure S4. The surface tension of octyl-OS is  
436 much lower than that of pure water, leading to significant reduction in critical supersaturations and  
437 thus overestimation of its  $\kappa_{ccn}$  value; for comparison, the surface tension depression is also visible  
438 but much less pronounced for octyl-OS/AS mixed aerosol. Overall, we proposed that solubility  
439 limit and surface tension reduction may both contribute to the observed discrepancy between  $\kappa_{gf}$   
440 and  $\kappa_{ccn}$  values for octyl-OS aerosol. We note that some numerical models (Petters and  
441 Kreidenweis, 2008, 2013; Riipinen et al., 2015) are available to quantitatively assess contribution  
442 of solubility limit and surface tension reduction to the discrepancy between  $\kappa_{gf}$  and  $\kappa_{ccn}$ .

#### 443 **4. Conclusions**

444 Organosulfates (OS) may contribute significantly to secondary organic aerosols in various  
445 locations over the globe; however, their hygroscopic properties and CCN activities have not been  
446 well understood. In this work, three complementary techniques, including a vapor sorption  
447 analyzer (VSA), a hygroscopicity tandem differential mobility analyzer (H-TDMA) and a cloud  
448 condensation nuclei counter (CCNc), were employed to investigate interactions of several OS with

449 water vapor under sub- and supersaturated conditions, trying to get a comprehensive picture of  
450 their hygroscopic properties and CCN activities.

451 VSA was used to measure mass change of OS samples with RH (0-90%). Obvious  
452 deliquescence was found for sodium methyl sulfate (methyl-OS), sodium ethyl sulfate (ethyl-OS),  
453 sodium octyl sulfate (octyl-OS) and potassium hydroxyacetone sulfate, and their mass growth  
454 factors at 90% RH were determined to be  $3.65 \pm 0.06$ ,  $3.58 \pm 0.02$ ,  $1.59 \pm 0.01$  and  $2.20 \pm 0.03$ ,  
455 respectively. No significant water uptake were observed up to 90% RH for other OS compounds  
456 examined, including sodium dodecyl sulfate, potassium 3-hydroxy phenyl sulfate, potassium  
457 benzyl sulfate, potassium 2-methyl benzyl sulfate, potassium 3-methyl benzyl sulfate, potassium  
458 2,4-dimethyl benzyl sulfate and potassium 3,5-dimethyl benzyl sulfate. Hygroscopic properties of  
459 methyl-, ethyl- and octyl-OS aerosols were also studied using H-TDMA, which measured mobility  
460 diameters of aerosol particles as a function of RH. Continuous hygroscopic growth was observed  
461 for methyl-, ethyl- and octyl-OS aerosols, and their growth factors at 90% RH were measured to  
462 be  $1.83 \pm 0.03$ ,  $1.79 \pm 0.02$  and  $1.21 \pm 0.02$ .

463 We further investigated CCN activities of methyl-, ethyl- and octyl-OS aerosols, and their  
464 single hygroscopicity parameters,  $\kappa_{\text{ccn}}$ , were determined to be  $0.459 \pm 0.021$ ,  $0.397 \pm 0.010$  and  
465  $0.206 \pm 0.008$ , respectively. For methyl- and ethyl-OS aerosols, single hygroscopicity parameters  
466 derived from CCN activities ( $\kappa_{\text{ccn}}$ ) agree reasonably well with those derived from H-TDMA  
467 measurements ( $\kappa_{\text{gf}}$ ) with relative differences being  $< 25\%$ . However,  $\kappa_{\text{ccn}}$  was found to be  $\sim 2.4$   
468 times larger than  $\kappa_{\text{gf}}$  for octyl-OS, and we show that solubility limit and surface tension reduction  
469 may both contribute to such discrepancy observed.

470

471 **Data availability.** Data used in this paper can be found in the main text or supplement.

472 **Competing interests.** The authors declare that they have no conflict of interest.

473 **Author contribution.** Mingjin Tang conceived this work; Ru-Jin Huang, Yuqing Zhang, Xiang  
474 Ding and Xinming Wang chose and provided samples investigated in this work; Chao Peng,  
475 Lanxiadi Chen, Yuqing Zhang and Xiang Ding conducted VSA measurements; Chao Peng,  
476 Weigang Wang and Maofa Ge conducted H-TDMA measurements; Patricia N. Razafindrambinina,  
477 Kotiba A. Malek and Akua A. Asa-Awuku conducted CCN activity measurements; Chao Peng,  
478 Patricia N. Razafindrambinina, Kotiba A. Malek, Akua A. Asa-Awuku and Mingjin Tang analyzed  
479 the data and prepared the manuscript with contribution from all the other coauthors.

#### 480 **Financial support**

481 This work was funded by National Natural Science Foundation of China (91744204), China  
482 Postdoctoral Science Foundation (2020M682931), Ministry of Science and Technology of China  
483 (2018YFC0213901), Chinese Academy of Sciences international collaborative project  
484 (132744KYSB20160036), State Key Laboratory of Loess and Quaternary Geology  
485 (SKLLQG1921), Guangdong Foundation for Program of Science and Technology Research  
486 (2019B121205006 and 2020B1212060053), Guangdong Science and Technology Department  
487 (2017GC010501) and CAS Pioneer Hundred Talents program.

488

#### 489 **References**

- 490 Brooks, S.: Water uptake by particles containing humic materials and mixtures of humic materials with ammonium  
491 sulfate, *Atmos. Environ.*, 38, 1859-1868, 2004.
- 492 Bruggemann, M., Xu, R., Tilgner, A., Kwong, K. C., Mutzel, A., Poon, H. Y., Otto, T., Schaefer, T., Poulain, L., Chan,  
493 M. N., and Herrmann, H.: Organosulfates in ambient aerosol: State of knowledge and future research directions on  
494 formation, abundance, fate, and importance, *Environ. Sci. Technol.*, 54, 3767-3782, 2020.
- 495 Chemistry Dashboard: United States Environmental Protection Agency, available at:  
496 <https://comptox.epa.gov/dashboard>, last access: 12 January 2021.
- 497 Chen, L., Chen, Y., Chen, L., Gu, W., Peng, C., Luo, S., Song, W., Wang, Z., and Tang, M.: Hygroscopic properties  
498 of 11 pollen species in China, *ACS Earth Space Chem.*, 3, 2678-2683, 2019.
- 499 Choi, M. Y., and Chan, C. K.: The effects of organic species on the hygroscopic behaviors of inorganic aerosols,  
500 *Environ. Sci. Technol.*, 36, 2422-2428, 2002.

501 Clegg, S. L., and Brimblecombe, P.: Equilibrium partial pressures of strong acids over concentrated saline solutions-  
502 1. HNO<sub>3</sub>, *Atmos. Environ.*, 22, 91-100, 1988.

503 Clegg, S. L., Brimblecombe, P., and Wexler, A. S.: Thermodynamic model of the system H<sup>+</sup>-NH<sub>4</sub><sup>+</sup>-Na<sup>+</sup>-SO<sub>4</sub><sup>2-</sup>-NO<sub>3</sub><sup>-</sup>-  
504 Cl-H<sub>2</sub>O at 298.15 K, *J. Phys. Chem. A*, 102, 2155-2171, 1998.

505 Ervens, B., Turpin, B., and Weber, R.: Secondary organic aerosol formation in cloud droplets and aqueous particles  
506 (aqSOA): a review of laboratory, field and model studies, *Atmos. Chem. Phys.*, 11, 11069-11102, 2011.

507 Estillore, A. D., Hettiyadura, A. P. S., Qin, Z., Leckrone, E., Wombacher, B., Humphry, T., Stone, E. A., and Grassian,  
508 V. H.: Water uptake and hygroscopic growth of organosulfate aerosol, *Environ. Sci. Technol.*, 50, 4259-4268, 2016.

509 Estillore, A. D., Morris, H. S., Or, V. W., Lee, H. D., Alves, M. R., Marciano, M. A., Laskina, O., Qin, Z., Tivanski,  
510 A. V., and Grassian, V. H.: Linking hygroscopicity and the surface microstructure of model inorganic salts, simple  
511 and complex carbohydrates, and authentic sea spray aerosol particles, *Phys. Chem. Chem. Phys.*, 19, 21101-21111,  
512 2017.

513 Froyd, K. D., Murphy, S. M., Murphy, D. M., de Gouw, J. A., Eddingsaas, N. C., and Wennberg, P. O.: Contribution  
514 of isoprene-derived organosulfates to free tropospheric aerosol mass, *P. Natl. Acad. Sci. USA*, 107, 21360-21365,  
515 2010.

516 Gu, W., Li, Y., Zhu, J., Jia, X., Lin, Q., Zhang, G., Ding, X., Song, W., Bi, X., Wang, X., and Tang, M.: Investigation  
517 of water adsorption and hygroscopicity of atmospherically relevant particles using a commercial vapor sorption  
518 analyzer, *Atmos. Meas. Tech.*, 10, 3821-3832, 2017.

519 Guo, L., Gu, W., Peng, C., Wang, W., Li, Y. J., Zong, T., Tang, Y., Wu, Z., Lin, Q., Ge, M., Zhang, G., Hu, M., Bi,  
520 X., Wang, X., and Tang, M.: A comprehensive study of hygroscopic properties of calcium- and magnesium-  
521 containing salts: Implication for hygroscopicity of mineral dust and sea salt aerosols, *Atmos. Chem. Phys.*, 2115-  
522 2133, 2019.

523 Hallquist, M., Wenger, J. C., Baltensperger, U., Rudich, Y., Simpson, D., Claeys, M., Dommen, J., Donahue, N. M.,  
524 George, C., Goldstein, A. H., Hamilton, J. F., Herrmann, H., Hoffmann, T., Iinuma, Y., Jang, M., Jenkin, M. E.,  
525 Jimenez, J. L., Kiendler-Scharr, A., Maenhaut, W., McFiggans, G., Mentel, T. F., Monod, A., Prevot, A. S. H.,  
526 Seinfeld, J. H., Surratt, J. D., Szmigielski, R., and Wildt, J.: The formation, properties and impact of secondary  
527 organic aerosol: Current and emerging issues, *Atmos. Chem. Phys.*, 9, 5155-5236, 2009.

528 Hansen, A. M. K., Kristensen, K., Nguyen, Q. T., Zare, A., Cozzi, F., Nojgaard, J. K., Skov, H., Brandt, J., Christensen,  
529 J. H., Strom, J., Tunved, P., Krejci, R., and Glasius, M.: Organosulfates and organic acids in Arctic aerosols:  
530 speciation, annual variation and concentration levels, *Atmos. Chem. Phys.*, 14, 7807-7823, 2014.

531 Hansen, A. M. K., Hong, J., Raatikainen, T., Kristensen, K., Ylisirnio, A., Virtanen, A., Petaja, T., Glasius, M., and  
532 Prisle, N. L.: Hygroscopic properties and cloud condensation nuclei activation of limonene-derived organosulfates  
533 and their mixtures with ammonium sulfate, *Atmos. Chem. Phys.*, 15, 14071-14089, 2015.

534 He, Q.-F., Ding, X., Wang, X.-M., Yu, J.-Z., Fu, X.-X., Liu, T.-Y., Zhang, Z., Xue, J., Chen, D.-H., Zhong, L.-J., and  
535 Donahue, N. M.: Organosulfates from pinene and isoprene over the Pearl River Delta, south China: Seasonal  
536 variation and implication in formation mechanisms, *Environ. Sci. Technol.*, 48, 9236-9245, 2014.

537 Heald, C. L., Jacob, D. J., Park, R. J., Russell, L. M., Huebert, B. J., Seinfeld, J. H., Liao, H., and Weber, R. J.: A large  
538 organic aerosol source in the free troposphere missing from current models, *Geophys. Res. Lett.*, 32, L18809, 2005.

539 Hettiyadura, A. P. S., Stone, E. A., Kundu, S., Baker, Z., Geddes, E., Richards, K., and Humphry, T.: Determination  
540 of atmospheric organosulfates using HILIC chromatography with MS detection, *Atmos. Meas. Tech.*, 8, 2347-2358,  
541 2015.

542 Hettiyadura, A. P. S., Jayarathne, T., Baumann, K., Goldstein, A. H., de Gouw, J. A., Koss, A., Keutsch, F. N., Skog,  
543 K., and Stone, E. A.: Qualitative and quantitative analysis of atmospheric organosulfates in Centreville, Alabama,  
544 *Atmos. Chem. Phys.*, 17, 1343-1359, 2017.

545 Huang, R.-J., Cao, J., Chen, Y., Yang, L., Shen, J., You, Q., Wang, K., Lin, C., Xu, W., Gao, B., Li, Y., Chen, Q.,  
546 Hoffmann, T., O'Dowd, C. D., Bilde, M., and Glasius, M.: Organosulfates in atmospheric aerosol: Synthesis and  
547 quantitative analysis of PM<sub>2.5</sub> from Xi'an, northwestern China, *Atmos. Meas. Tech.*, 11, 3447-3456, 2018.

548 Hughes, D. D., and Stone, E. A.: Organosulfates in the Midwestern United States: Abundance, composition and  
549 stability, *Environ. Chem.*, 16, 312-322, 2019.

550 Jimenez, J., Canagaratna, M., Donahue, N., Prevot, A., Zhang, Q., Kroll, J. H., DeCarlo, P. F., Allan, J. D., Coe, H.,  
551 and Ng, N.: Evolution of organic aerosols in the atmosphere, *Science*, 326, 1525-1529, 2009.

552 Jing, B., Tong, S., Liu, Q., Li, K., Wang, W., Zhang, Y., and Ge, M.: Hygroscopic behavior of multicomponent organic  
553 aerosols and their internal mixtures with ammonium sulfate, *Atmos. Chem. Phys.*, 16, 4101-4118, 2016.

554 Kanakidou, M., Seinfeld, J., Pandis, S., Barnes, I., Dentener, F., Facchini, M., Dingenen, R. V., Ervens, B., Nenes, A.,  
555 and Nielsen, C.: Organic aerosol and global climate modelling: A review, *Atmos. Chem. Phys.*, 5, 1053-1123, 2005.

556 Kreidenweis, S. M., Koehler, K., DeMott, P. J., Prenni, A. J., Carrico, C., and Ervens, B.: Water activity and activation  
557 diameters from hygroscopicity data - Part I: Theory and application to inorganic salts, *Atmos. Chem. Phys.*, 5, 1357-  
558 1370, 2005.

559 Kristensen, K., and Glasius, M.: Organosulfates and oxidation products from biogenic hydrocarbons in fine aerosols  
560 from a forest in North West Europe during spring, *Atmos. Environ.*, 45, 4546-4556, 2011.

561 Kundu, S., Quraishi, T. A., Yu, G., Suarez, C., Keutsch, F. N., and Stone, E. A.: Evidence and quantitation of aromatic  
562 organosulfates in ambient aerosols in Lahore, Pakistan, *Atmos. Chem. Phys.*, 13, 4865-4875, 2013.

563 Kwong, K. C., Chim, M. M., Davies, J. F., Wilson, K. R., and Chan, M. N.: Importance of sulfate radical anion  
564 formation and chemistry in heterogeneous OH oxidation of sodium methyl sulfate, the smallest organosulfate,  
565 *Atmos. Chem. Phys.*, 18, 2809-2820, 2018.

566 Lance, S., Medina, J., Smith, J. N., and Nenes, A.: Mapping the operation of the DMT Continuous Flow CCN counter,  
567 *Aerosol Sci. Tech.*, 40, 242-254, 2006.

568 Lei, T., Zuend, A., Wang, W. G., Zhang, Y. H., and Ge, M. F.: Hygroscopicity of organic compounds from biomass  
569 burning and their influence on the water uptake of mixed organic ammonium sulfate aerosols, *Atmos. Chem. Phys.*,  
570 14, 11165-11183, 2014.

571 Liao, J., Froyd, K. D., Murphy, D. M., Keutsch, F. N., Yu, G., Wennberg, P. O., St. Clair, J. M., Crouse, J. D.,  
572 Wisthaler, A., Mikoviny, T., Jimenez, J. L., Campuzano-Jost, P., Day, D. A., Hu, W., Ryerson, T. B., Pollack, I. B.,  
573 Peischl, J., Anderson, B. E., Ziemba, L. D., Blake, D. R., Meinardi, S., and Diskin, G.: Airborne measurements of  
574 organosulfates over the continental US, *J. Geophys. Res.-Atmos.*, 120, 2990-3005, 2015.

575 Ling, T. Y., and Chan, C. K.: Partial crystallization and deliquescence of particles containing ammonium sulfate and  
576 dicarboxylic acids, *J. Geophys. Res.-Atmos.*, 113, 2008.

577 Ma, Y., Xu, X., Song, W., Geng, F., and Wang, L.: Seasonal and diurnal variations of particulate organosulfates in  
578 urban Shanghai, China, *Atmos. Environ.*, 85, 152-160, 2014.

579 Malm, W. C., and Kreidenweis, S. M.: The effects of models of aerosol hygroscopicity on the apportionment of  
580 extinction, *Atmos. Environ.*, 31, 1965-1976, 1997.

581 Marcolli, C., and Krieger, U. K.: Phase changes during hygroscopic cycles of mixed organic/inorganic model systems  
582 of tropospheric aerosols, *J. Phys. Chem. A*, 110, 1881-1893, 2006.

583 McNeill, V. F., Woo, J. L., Kim, D. D., Schwier, A. N., Wannell, N. J., Sumner, A. J., and Barakat, J. M.: Aqueous-  
584 phase secondary organic aerosol and organosulfate formation in atmospheric aerosols: A modeling study, *Environ.*  
585 *Sci. Technol.*, 46, 8075-8081, 2012.

586 Mikhailov, E., Vlasenko, S., Martin, S. T., Koop, T., and Poeschl, U.: Amorphous and crystalline aerosol particles  
587 interacting with water vapor: conceptual framework and experimental evidence for restructuring, phase  
588 transitions and kinetic limitations, *Atmos. Chem. Phys.*, 9, 9491-9522, 2009.

589 Moise, T., Flores, J. M., and Rudich, Y.: Optical properties of secondary organic aerosols and their changes by  
590 chemical processes, *Chem. Rev.*, 115, 4400-4439, 2015.

591 Moore, R. H., Nenes, A., and Medina, J.: Scanning mobility CCN analysis-a method for fast measurements of size-  
592 resolved CCN distributions and activation kinetics, *Aerosol Sci. Tech.*, 44, 861-871, 2010.

593 Noziere, B., Kaberer, M., Claeys, M., Allan, J., D'Anna, B., Decesari, S., Finessi, E., Glasius, M., Grgic, I., Hamilton,  
594 J. F., Hoffmann, T., Iinuma, Y., Jaoui, M., Kahno, A., Kampf, C. J., Kourtschev, I., Maenhaut, W., Marsden, N.,  
595 Saarikoski, S., Schnelle-Kreis, J., Surratt, J. D., Szidat, S., Szmigielski, R., and Wisthaler, A.: The molecular  
596 identification of organic compounds in the atmosphere: State of the art and challenges, *Chem. Rev.*, 115, 3919-  
597 3983, 2015.

598 Pöschl, U.: Atmospheric aerosols: Composition, transformation, climate and health effects, *Angew. Chem. Int. Edit.*,  
599 44, 7520-7540, 2005.

600 Peng, C., Jing, B., Guo, Y. C., Zhang, Y. H., and Ge, M. F.: Hygroscopic behavior of multicomponent aerosols  
601 involving NaCl and dicarboxylic acids, *J. Phys. Chem. A*, 120, 1029-1038, 2016.

602 Peng, C., Wang, Y., Wu, Z., Chen, L., Huang, R. J., Wang, W., Wang, Z., Hu, W., Zhang, G., Ge, M., Hu, M., Wang,  
603 X., and Tang, M.: Tropospheric aerosol hygroscopicity in China, *Atmos. Chem. Phys.*, 20, 13877-13903, 2020.

604 Petters, M. D., and Kreidenweis, S. M.: A single parameter representation of hygroscopic growth and cloud  
605 condensation nucleus activity, *Atmos. Chem. Phys.*, 7, 1961-1971, 2007.

606 Petters, M. D., and Kreidenweis, S. M.: A single parameter representation of hygroscopic growth and cloud  
607 condensation nucleus activity - Part 2: Including solubility, *Atmos. Chem. Phys.*, 8, 6273-6279, 2008.

608 Petters, M. D., Wex, H., Carrico, C. M., Hallbauer, E., Massling, A., McMeeking, G. R., Poulain, L., Wu, Z.,  
609 Kreidenweis, S. M., and Stratmann, F.: Towards closing the gap between hygroscopic growth and activation for  
610 secondary organic aerosol - Part 2: Theoretical approaches, *Atmos. Chem. Phys.*, 9, 3999-4009, 2009.

611 Petters, M. D., and Kreidenweis, S. M.: A single parameter representation of hygroscopic growth and cloud  
 612 condensation nucleus activity - Part 3: Including surfactant partitioning, *Atmos. Chem. Phys.*, 13, 1081-1091, 2013.  
 613 Pitzer, K. S., and Mayorga, G.: Thermodynamics of electrolytes. 2. Activity and osmotic coefficients for strong  
 614 electrolytes with one or both ions univalent, *J. Phys. Chem.*, 77, 2300-2308, 1973.  
 615 Prenni, A.: Water uptake of internally mixed particles containing ammonium sulfate and dicarboxylic acids, *Atmos.*  
 616 *Environ.*, 37, 4243-4251, 2003.  
 617 Riipinen, I., Rastak, N., and Pandis, S. N.: Connecting the solubility and CCN activation of complex organic aerosols:  
 618 A theoretical study using solubility distributions, *Atmos. Chem. Phys.*, 15, 6305-6322, 2015.  
 619 Riva, M., Chen, Y., Zhang, Y., Lei, Z., Olson, N. E., Boyer, H. C., Narayan, S., Yee, L. D., Green, H. S., Cui, T.,  
 620 Zhang, Z., Baumann, K., Fort, M., Edgerton, E., Budisulistiorini, S. H., Rose, C. A., Ribeiro, I. O., RL, E. O., Dos  
 621 Santos, E. O., Machado, C. M. D., Szopa, S., Zhao, Y., Alves, E. G., de Sa, S. S., Hu, W., Knipping, E. M., Shaw,  
 622 S. L., Duvoisin Junior, S., de Souza, R. A. F., Palm, B. B., Jimenez, J. L., Glasius, M., Goldstein, A. H., Pye, H. O.  
 623 T., Gold, A., Turpin, B. J., Vizuete, W., Martin, S. T., Thornton, J. A., Dutcher, C. S., Ault, A. P., and Surratt, J.  
 624 D.: Increasing isoprene epoxydiol-to-inorganic sulfate aerosol ratio results in extensive conversion of inorganic  
 625 sulfate to organosulfur forms: Implications for aerosol physicochemical properties, *Environ. Sci. Technol.*, 53, 8682-  
 626 8694, 2019.  
 627 Roberts, G. C., and Nenes, A.: A continuous-flow streamwise thermal-gradient CCN chamber for atmospheric  
 628 measurements, *Aerosol Sci. Tech.*, 39, 206-221, 2005.  
 629 Shrivastava, M., Cappa, C. D., Fan, J., Goldstein, A. H., Guenther, A. B., Jimenez, J. L., Kuang, C., Laskin, A., Martin,  
 630 S. T., Ng, N. L., Petaja, T., Pierce, J. R., Rasch, P. J., Roldin, P., Seinfeld, J. H., Shilling, J., Smith, J. N., Thornton,  
 631 J. A., Volkamer, R., Wang, J., Worsnop, D. R., Zaveri, R. A., Zelenyuk, A., and Zhang, Q.: Recent advances in  
 632 understanding secondary organic aerosol: Implications for global climate forcing, *Rev. Geophys.*, 55, 509-559,  
 633 2017.  
 634 Staudt, S., Kundu, S., Lehmler, H.-J., He, X., Cui, T., Lin, Y.-H., Kristensen, K., Glasius, M., Zhang, X., Weber, R.  
 635 J., Surratt, J. D., and Stone, E. A.: Aromatic organosulfates in atmospheric aerosols: Synthesis, characterization,  
 636 and abundance, *Atmos. Environ.*, 94, 366-373, 2014.  
 637 Stokes, R. H., and Robinson, R. A.: Interactions in aqueous nonelectrolyte solutions. I. Solute-solvent equilibria, *J.*  
 638 *Phys. Chem.*, 70, 2126-2131, 1966.  
 639 Surratt, J. D., Gomez-Gonzalez, Y., Chan, A. W. H., Vermeylen, R., Shahgholi, M., Kleindienst, T. E., Edney, E. O.,  
 640 Offenberg, J. H., Lewandowski, M., Jaoui, M., Maenhaut, W., Claeys, M., Flagan, R. C., and Seinfeld, J. H.:  
 641 Organosulfate formation in biogenic secondary organic aerosol, *J. Phys. Chem. A*, 112, 8345-8378, 2008.  
 642 Svenningsson, B., Rissler, J., Swietlicki, E., Mircea, M., Bilde, M., Facchini, M. C., Decesari, S., Fuzzi, S., Zhou, J.,  
 643 Monster, J., and Rosenorn, T.: Hygroscopic growth and critical supersaturations for mixed aerosol particles of  
 644 inorganic and organic compounds of atmospheric relevance, *Atmos. Chem. Phys.*, 6, 1937-1952, 2006.  
 645 Tang, M., Cziczo, D. J., and Grassian, V. H.: Interactions of water with mineral dust aerosol: Water adsorption,  
 646 hygroscopicity, cloud condensation, and ice nucleation, *Chem. Rev.*, 116, 4205-4259, 2016.  
 647 Tang, M., Chan, C. K., Li, Y. J., Su, H., Ma, Q., Wu, Z., Zhang, G., Wang, Z., Ge, M., Hu, M., He, H., and Wang, X.:  
 648 A review of experimental techniques for aerosol hygroscopicity studies, *Atmos. Chem. Phys.*, 19, 12631-12686,  
 649 2019a.  
 650 Tang, M., Gu, W., Ma, Q., Li, Y. J., Zhong, C., Li, S., Yin, X., Huang, R.-J., He, H., and Wang, X.: Water adsorption  
 651 and hygroscopic growth of six anemophilous pollen species: the effect of temperature, *Atmos. Chem. Phys.*, 19,  
 652 2247-2258, 2019b.  
 653 Tolocka, M. P., and Turpin, B.: Contribution of organosulfur compounds to organic aerosol mass, *Environ. Sci.*  
 654 *Technol.*, 46, 7978-7983, 2012.  
 655 Wang, K., Zhang, Y., Huang, R.-J., Wang, M., Ni, H., Kampf, C. J., Cheng, Y., Bilde, M., Glasius, M., and Hoffmann,  
 656 T.: Molecular characterization and source identification of atmospheric particulate organosulfates using ultrahigh  
 657 resolution mass spectrometry, *Environ. Sci. Technol.*, 53, 6192-6202, 2019a.  
 658 Wang, Y., Hu, M., Guo, S., Wang, Y., Zheng, J., Yang, Y., Zhu, W., Tang, R., Li, X., Liu, Y., Le Breton, M., Du, Z.,  
 659 Shang, D., Wu, Y., Wu, Z., Song, Y., Lou, S., Hallquist, M., and Yu, J.: The secondary formation of organosulfates  
 660 under interactions between biogenic emissions and anthropogenic pollutants in summer in Beijing, *Atmos. Chem.*  
 661 *Phys.*, 18, 10693-10713, 2018.  
 662 Wang, Y., Ma, Y., Li, X., Kuang, B. Y., Huang, C., Tong, R., and Yu, J. Z.: Monoterpene and sesquiterpene alpha-  
 663 hydroxy organosulfates: Synthesis, MS/MS characteristics, and ambient presence, *Environ. Sci. Technol.*, 53,  
 664 12278-12290, 2019b.

665 Wang, Y., Hu, M., Wang, Y.-C., Li, X., Fang, X., Tang, R., Lu, S., Wu, Y., Guo, S., Wu, Z., Hallquist, M., and Yu,  
666 J. Z.: Comparative study of particulate organosulfates in contrasting atmospheric environments: Field evidence for  
667 the significant influence of anthropogenic sulfate and NO<sub>x</sub>, *Environ. Sci. Technol. Lett.*, 7, 787-794, 2020.

668 Wang, Y., Zhao, Y., Wang, Y., Yu, J. Z., Shao, J., Liu, P., Zhu, W., Cheng, Z., Li, Z., Yan, N., and Xiao, H.:  
669 Organosulfates in atmospheric aerosols in Shanghai, China: Seasonal and interannual variability, origin, and  
670 formation mechanisms, *Atmos. Chem. Phys.*, 21, 2959-2980, 2021.

671 Wex, H., Petters, M., Carrico, C., Hallbauer, E., Massling, A., McMeeking, G., Poulain, L., Wu, Z., Kreidenweis, S.,  
672 and Stratmann, F.: Towards closing the gap between hygroscopic growth and activation for secondary organic  
673 aerosol: Part 1—Evidence from measurements, *Atmos. Chem. Phys.*, 9, 3987-3997, 2009.

674 Wexler, A. S., and Clegg, S. L.: Atmospheric aerosol models for systems including the ions H<sup>+</sup>, NH<sub>4</sub><sup>+</sup>, Na<sup>+</sup>, SO<sub>4</sub><sup>2-</sup>,  
675 NO<sub>3</sub><sup>-</sup>, Cl<sup>-</sup>, Br<sup>-</sup>, and H<sub>2</sub>O, *J. Geophys. Res.-Atmos.*, 107, 4207, 2002.

676 Wiedensohler, A., Birmili, W., Nowak, A., Sonntag, A., Weinhold, K., Merkel, M., Wehner, B., Tuch, T., Pfeifer, S.,  
677 Fiebig, M., Fjaraa, A. M., Asmi, E., Sellegri, K., Depuy, R., Venzac, H., Villani, P., Laj, P., Aalto, P., Ogren, J. A.,  
678 Swietlicki, E., Williams, P., Roldin, P., Quincey, P., Hueglin, C., Fierz-Schmidhauser, R., Gysel, M., Weingartner,  
679 E., Riccobono, F., Santos, S., Gruening, C., Faloony, K., Beddows, D., Harrison, R. M., Monahan, C., Jennings, S.  
680 G., O'Dowd, C. D., Marinoni, A., Horn, H. G., Keck, L., Jiang, J., Scheckman, J., McMurry, P. H., Deng, Z., Zhao,  
681 C. S., Moerman, M., Henzing, B., de Leeuw, G., Loeschau, G., and Bastian, S.: Mobility particle size spectrometers:  
682 harmonization of technical standards and data structure to facilitate high quality long-term observations of  
683 atmospheric particle number size distributions, *Atmos. Meas. Tech.*, 5, 657-685, 2012.

684 Wise, M. E., Surratt, J. D., Curtis, D. B., Shilling, J. E., and Tolbert, M. A.: Hygroscopic growth of ammonium  
685 sulfate/dicarboxylic acids, *J. Geophys. Res.-Atmos.*, 108, 4638, 2003.

686 Wu, Z. J., Nowak, A., Poulain, L., Herrmann, H., and Wiedensohler, A.: Hygroscopic behavior of atmospherically  
687 relevant water-soluble carboxylic salts and their influence on the water uptake of ammonium sulfate, *Atmospheric  
688 Chemistry and Physics*, 11, 12617-12626, 2011.

689 Zardini, A. A., Sjogren, S., Marcolli, C., Krieger, U. K., Gysel, M., Weingartner, E., Baltensperger, U., and Peter, T.:  
690 A combined particle trap/HTDMA hygroscopicity study of mixed inorganic/organic aerosol particles, *Atmos. Chem.  
691 Phys.*, 8, 5589-5601, 2008.

692 Zhang, Y.-Q., Chen, D.-H., Ding, X., Li, J., Zhang, T., Wang, J.-Q., Cheng, Q., Jiang, H., Song, W., Ou, Y.-B., Ye,  
693 P.-L., Zhang, G., and Wang, X.-M.: Impact of anthropogenic emissions on biogenic secondary organic aerosol:  
694 observation in the Pearl River Delta, southern China, *Atmos. Chem. Phys.*, 19, 14403-14415, 2019.

695